INTERNATIONAL JOURNAL FOR NUMERICAL METHODS IN FLUIDS
Int. J. Numer. Meth. Fluids **28**: 267–291 (1998)

COMPUTATIONS USING THE PRECONDITIONING BI-CGSTAB ALGORITHM IN CHEMICAL NON-EQUILIBRIUM PROBLEMS

HERNG LIN[a] AND CHING-CHANG CHIENG[b,*]

[a] *Chung Shan Institute of Science and Technology, Lung-Tan Box 90008-15-5, Tauyung 32526, Taiwan, Republic of China*
[b] *Department of Nuclear Engineering, National Tsing Hua University, Hsinchu, 30043, Taiwan, Republic of China*

SUMMARY

A robust method for solving the chemical non-equilibrium Navier–Stokes equations, including all of the species conservation and energy production equations, is developed. The algorithm is embodied in a fully coupled, implicit, large block structure. Van Leer flux splitting for inviscid terms and central differencing for viscous terms in the explicit operators are applied in the numerical algorithm. The fully-coupled system is solved implicitly and the bi-conjugate gradient stable (Bi-CGSTAB) method with a preconditioner of incomplete lower–upper (LU)-factorization (ILU) is used for solving large block structure and diagonal dominate matrix equations. The computations are performed for the hypersonic inflow over blunt bodies including half cylinder, double ellipse and blunt nose. The adaptive grid constructed by moving grid method is employed to capture the shock location. Computational results in the present study are compared with other calculated data and exhibit good agreement. Convergence histories of the mean flow variables and species equations demonstrate that the fast convergent rate can be achieved by the preconditioned Bi-CGSTAB method. © 1998 John Wiley & Sons, Ltd.

KEY WORDS: non-equilibrium equations; Bi-CGSTAB method; adaptive grid

1. INTRODUCTION

The computation of high speed flow with non-equilibrium chemistry and thermodynamics has been an interesting subject in recent years. The large number of dependent variables and additional species transport equations with large source term, and the disparate time scales associated with the fluid motion and non-equilibrium chemistry and thermodynamics make the corresponding equation set very stiff. Maximizing accuracy, efficiency, and robustness of the numerical method is the first goal. In recent years, numerous investigators [1–6] derived flux splitting methods for inviscid terms of the compressible flow equations for gases that are not in chemical equilibrium. Usually, formulas are proposed so that the methods can be extended to chemical non-equilibrium, by Steger–Warming [7] and Van Leer flux vector splittings [8], and Roe flux difference splitting [9]. The major difficulty for developing the flux splitting algorithm for real gas in chemical equilibrium and non-equilibrium is that the Euler equations will not be homogeneous of degree one, as is the case for a perfect gas, which indicates that the existing perfect gas flux split algorithm is not applicable. Formulas are derived by two

* Correspondence to: Department of Nuclear Engineering, National Tsing Hua University, Hsinchu 30043, Taiwan, Republic of China.

CCC 0271–2091/98/120267–25$17.50

Received January 1997
Revised April 1997

approaches: 'equivalent γ' method and a more complicate flux splitting [2–6]. The 'equivalent γ' method, first suggested by Grossman and Walters [1] for flow in chemical non-equilibrium, was developed by Desideri [10], Shuen [11] and Mani [12], and is used in the present study.

For flow with very significant non-equilibrium effects and large thermal energy changes due to heat release or absorption, all the equations are solved in a simultaneous, coupled manner. Therefore, the solution algorithm needs to be devised with this large block structure. In general, the implicit scheme can enlarge the integrating time step and be robust, but the memory and CPU are considerable, especially for 3-D calculation. Palmer [13] designed a 3-D explicit finite rate code to compute AFE vehicle flow in chemical non-equilibrium. The necessary underrelaxation process was suggested because otherwise the CFL number may be restricted by very stiff source terms and may be less than 0.0001. To accelerate the convergence rate, many existing factored implicit algorithms are implemented for chemical non-equilibrium flow, such as lower–upper (LU) [14,15], ADI [15], LU-SSOR [11], LU-SGS [16], diagonalized ADI [12], etc. The source term of chemical production was treated implicitly to overcome the stiff property. In relation to flux Jacobian for inviscid flux of transport equations, the source term Jacobian matrix can be similarly derived [3]. Unfortunately, the source term Jacobian matrix element has a broad value (i.e. the value may be positive or negative, the absolute value may be very large or approach zero) and is not diagonal dominated. So the diagonal scheme (for example, diagonalized ADI, LU-SGS, LU-SSOR, etc.) for chemical non-equilibrium flow has been popular in recent years. The diagonal scheme eliminated the expense of inverting the large block matrices that arise when species conservation equations are introduced. A simplified approach to 'diagonalize' the source term Jacobian within the diagonalized implicit algorithm framework has been implemented and tested by Imaly *et al*. [17]. These formulations always add to the diagonal dominance of the implicit operator and thus will underrelax the effects of the chemical source term. But these algorithms may exhibit poor convergence behavior if the simplification of the source term Jacobian is not suitable. The non-diagonalized LU algorithm designed by Shuen [14] displays very good convergent behavior, and apparently is faster than the LU-SGS method for the same computational problem. Shuen [14] used the Van Leer flux splitting for inviscid terms and central differencing for viscous terms in the explicit operator, and Steger–Warming splitting LU approximate factorization for the implicit operator. However, the LU approximate factorization induces the factorization error. Gnoffo [18] used upwind-biased, point-implicit relaxation strategies to design the LAURA code for viscous hypersonic flow. Candler and MacCormack [19] used an implicit Gauss–Seidel line relaxation technique [20] to compute a two-dimensional hypersonic flow field that is ionized and in thermal–chemical non-equilibrium. The relaxation method needs iterations to obtain the solution of a large linear system and the problem of convergence needs to be resolved.

In recent years, the convergence has been greatly improved using the conjugate gradient (CG) method [21]. Preconditioned conjugate gradient, and its generalizations for non-symmetric systems such as Bi-CG [22], GCR [23] and the generalized minimal residual method (GMRES) [24], have been employed for many CFD codes [25,26]. Furthermore, Venkatakrishnan [27] used them to obtain solutions of the compressible Navier–Stokes equations for subsonic and transonic flows. Ajmani *et al*. [28] used the GMRES method of Saad and Schultz [24] for transonic and hypersonic flow with fast convergence. It was found that the conjugate gradient squared (CGS) method [29] was competitive in convergence acceleration with the GMRES method and was economical in both storage requirement and computing time. The bi-conjugate gradient stable (Bi-CGSTAB) method [30] exhibited a more stable convergence behavior than the CGS method and less CPU time with the same convergence behavior rate compared with the QMR [31] and TFQMR method [32]. The authors' previous studies [33,34]

have employed various Bi-CG variants to compute the transonic separated turbulent flow by adopting higher order turbulence models which have the same problem of stiffness.

For the present study, the preconditioned Bi-CGSTAB method [30] is implemented to the compressible Navier–Stokes solver with the non-equilibrium chemically reacting gas model. Satisfactory convergence behavior for the test problems of a half cylinder, a double ellipse and a blunt body will be demonstrated. In addition, Shuen's method is slightly modified to solve mean flow equations and species equations with five-species and 11-species chemical reaction models [35,36] of dissociated air.

2. MATHEMATICAL MODEL

2.1. Governing equations

Two-dimensional Navier–Stokes and species transport equations for a chemically reacting gas of N_s species can be formulated in curvilinear co-ordinate and written in non-dimensional form as follows:

$$\frac{\partial \hat{Q}}{\partial t}+\frac{\partial \hat{E}}{\partial \xi}+\frac{\partial \hat{F}}{\partial \eta}=\frac{\partial \hat{E}_v}{\partial \xi}+\frac{\partial \hat{F}_v}{\partial \eta}+\hat{S} \tag{1}$$

where $\hat{Q}$, $\hat{E}$, $\hat{F}$, $\hat{E}_v$, $\hat{F}_v$, $\hat{S}$ are $(N_s+3)\times 1$ column matrices and their elements are:

$$\hat{Q}=\frac{1}{J}\left[\rho, \rho u, \rho v, E_t, \rho_1, \rho_2, \ldots, \rho_{N_{s-1}}\right]$$

$$\hat{E}=\frac{1}{J}\begin{pmatrix} \rho U \\ \rho uU+\xi_x p \\ \rho vU+\xi_y p \\ U(E_t+p) \\ \rho_1 U \\ \rho_2 U \\ \vdots \\ \rho_{N_{s-1}} U \end{pmatrix} \qquad \hat{F}=\frac{1}{J}\begin{pmatrix} \rho V \\ \rho uV+\eta_x p \\ \rho vV+\eta_y p \\ V(E_t+p) \\ \rho_1 V \\ \rho_2 V \\ \vdots \\ \rho_{N_{s-1}} V \end{pmatrix} \tag{2}$$

$$\hat{E}_v=\frac{M_\infty}{Re_\infty J}\left[0, E_{v_2}, E_{v_3}, E_{v_4}, E_{v_5}, \ldots, E_{v_{N_s+3}}\right]^T \qquad \hat{F}_v=\frac{M_\infty}{Re_\infty J}\left[0, F_{v_2}, F_{v_3}, F_{v_4}, F_{v_5}, \ldots, F_{v_{N_s+3}}\right]^T$$

$$\hat{S}=\frac{1}{J}\left[0, 0, 0, 0, S_1, S_2, \ldots, S_{N_{s-1}}\right]^T$$

The terms in $\hat{E}_v$ and $\hat{F}_v$ are expressed as

$$E_{v_2}=\tau_{xx}\xi_x+\tau_{xy}\xi_y, \qquad E_{v_3}=\tau_{xy}\xi_x+\tau_{yy}\xi_y,$$

$$E_{v4}=u(\tau_{xx}\xi_x+\tau_{xy}\xi_y)+v(\tau_{xy}\xi_x+\tau_{yy}\xi_y)+\dot{q}_x\xi_x+\dot{q}_y\xi_y+\sum_{i=1}^{N_s-1}D_{im}h_i\left(\frac{\partial Y_i}{\partial x}\xi_x+\frac{\partial Y_i}{\partial y}\xi_y\right)$$

$$E_{v_5}=\frac{\partial Y_1}{\partial x}\xi_x+\frac{\partial Y_1}{\partial y}\xi_y, \qquad E_{v_{N_s+3}}=\frac{\partial Y_{N_s-1}}{\partial x}\xi_x+\frac{\partial Y_{N_s-1}}{\partial y}\xi_y,$$

$$F_{v_2}=\tau_{xx}\eta_x+\tau_{xy}\eta_y, \qquad F_{v_3}=\tau_{xy}\eta_x+\tau_{yy}\eta_y,$$

$$F_{v_4} = u(\tau_{xx}\eta_x + \tau_{xy}\eta_y) + v(\tau_{xy}\eta_x + \tau_{yy}\eta_y) + \dot{q}_x\eta_x + \dot{q}_y\eta_y + \sum_{i=1}^{N_s-1} D_{im}h_i\left(\frac{\partial Y_i}{\partial x}\eta_x + \frac{\partial Y_i}{\partial y}\eta_y\right)$$

$$F_{v_5} = \frac{\partial Y_1}{\partial x}\eta_x + \frac{\partial Y_1}{\partial y}\eta_y, \qquad F_{v_{N_s+3}} = \frac{\partial Y_{N_s-1}}{\partial x}\eta_x + \frac{\partial Y_{N_s-1}}{\partial y}\eta_y,$$

x, y are the Cartesian co-ordinates in longitudinal and radial directions, ξ, η are the transformed co-ordinates, and t is the time. $\rho_1, \rho_2, \ldots, \rho N_{s-1}, \rho N_s$ are the densities of each species. So the mixture density is

$$\rho = \rho_1 + \rho_2 + \cdots + \rho_{N_s-1} + \rho_{N_s} \tag{3}$$

and $Y_i \equiv \rho_i/\rho$ is the mass fraction for the ith species. u, v are the velocity components, ρ is the static pressure and E_t is the total energy. S_1 to $S_{N_{s-1}}$ are the source terms for species due to chemical reactions. Non-dimensionalized variables are:

$$\rho = \frac{\tilde{\rho}}{\tilde{\rho}_\infty}, \qquad u = \frac{\tilde{u}}{\tilde{a}_\infty}, \qquad v = \frac{\tilde{v}}{\tilde{a}_\infty}, \qquad a = \frac{\tilde{a}}{\tilde{a}_\infty}, \qquad p = \frac{\tilde{p}}{\tilde{\rho}_\infty \tilde{a}_\infty^2},$$

$$E_t = \frac{\tilde{E}_t}{\tilde{\rho}_\infty \tilde{a}_\infty^2}, \qquad e = \frac{\tilde{e}}{\tilde{a}_\infty^2}, \qquad h = \frac{\tilde{h}}{\tilde{\rho}_\infty \tilde{a}_\infty^2}, \qquad T = \frac{\tilde{T}}{\tilde{T}_\infty},$$

$$\mu = \frac{\tilde{\mu}}{\tilde{\mu}_\infty}, \qquad \kappa = \frac{\tilde{\kappa}}{\tilde{\kappa}_\infty}, \qquad Re_\infty = \frac{\tilde{\rho}_\infty \tilde{V}_\infty \tilde{L}_{\text{ref}}}{\tilde{\mu}_\infty} \qquad \rho_i = \frac{\tilde{\rho}_i}{\tilde{\rho}_\infty},$$

$$e_i = \frac{\tilde{e}_i}{\tilde{a}_\infty^2}, \qquad h_i = \frac{\tilde{h}_i}{\tilde{a}_\infty^2}, \qquad \mu_i = \frac{\tilde{\mu}_i}{\tilde{\mu}_\infty}, \qquad D_{im} = \frac{\tilde{D}_{im}\tilde{\rho}_\infty}{\tilde{\mu}_\infty}$$

where e is the specific internal energy, h is the specific enthalpy, a is the sound speed, T is the static temperature, μ is the molecular viscosity, κ is the thermal conductivity, Re_∞, is the freestream Reynolds number, and L_{ref} is reference length. The subscript i denotes the flow property of ith species. D_{im} is the effective binary diffusivity of species i in the mixture.

Also

$$J = \xi_x\eta_y - \xi_y\eta_x, \qquad U = \xi_x u + \xi_y v, \qquad V = \eta_x u + \eta_y v$$

$$\tau_{xx} = \frac{2}{3}\mu(2u_x - v_y), \qquad \tau_{yy} = \frac{2}{3}\mu(2v_x - u_y), \qquad \tau_{xy} = \mu(u_y + v_x)$$

$$\dot{q}_x = \left(\frac{\tilde{\kappa}_\infty \tilde{T}_\infty}{\tilde{\mu}_\infty \tilde{a}_\infty^2}\right)\left[\xi_x\frac{\partial T}{\partial \xi} + \eta_x\frac{\partial T}{\partial \eta}\right], \qquad \dot{q}_y = \left(\frac{\tilde{\kappa}_\infty \tilde{T}_\infty}{\tilde{\mu}_\infty \tilde{a}_\infty^2}\right)\left[\xi_y\frac{\partial T}{\partial \xi} + \eta_y\frac{\partial T}{\partial \eta}\right].$$

2.2. Transport properties

The molecular viscosities of each species are calculated by the Blottner [37] formula:

$$\tilde{\mu}_i = 0.1 \exp\left[(A_i \ln \tilde{T} + B_i)\ln \tilde{T} + C_i\right], \text{ kg m}^{-1}\text{ s}^{-1}. \tag{4}$$

The unit of $\tilde{T}$ is K, and A_i, B_i, C_i are Blottner coefficients [37]. Eucken's formula [38] is used to compute thermal conductivity:

$$\tilde{\kappa}_i = \frac{\tilde{\mu}_i R_u}{W_i}\left(\frac{c_{p,i} W_i}{R_u} + \frac{5}{4}\right). \tag{5}$$

The molecular viscosity and thermal conductivity of the gas mixture is calculated from Wilke's [39] law:

$$\tilde{\mu} = \sum_i \frac{\chi_i \tilde{\mu}_i}{\Sigma_j \chi_j \Phi_{ij}} \tag{6}$$

$$\tilde{\kappa} = \sum_i \frac{\chi_i \tilde{\kappa}_i}{\Sigma_j \chi_j \psi_{ij}}, \tag{7}$$

where χ_i is molar fraction of each species, i.e.

$$\chi_i = \frac{\rho_i W}{\rho W_i}, \tag{8}$$

where W, and W_i are the molecular weights of the gas mixture and ith species. Φ_{ij} and ψ_{ij}, are defined as

$$\Phi_{ij} = \frac{1}{\sqrt{8}}\left(1 + \frac{W_i}{W_j}\right)^{1/2}\left[1 + \left(\frac{\mu_i}{\mu_j}\right)^{1/2}\left(\frac{W_j}{W_i}\right)^{1/4}\right]$$
$$\psi_{ij} = \frac{1}{\sqrt{8}}\left(1 + \frac{W_i}{W_j}\right)^{1/2}\left[1 + \left(\frac{\kappa_i}{\kappa_j}\right)^{1/2}\left(\frac{W_j}{W_i}\right)^{1/4}\right]. \tag{9}$$

The effective diffusivity of species i in the gas mixture can be expressed by

$$D_{i\mathrm{m}} = (1 - \chi_i) \Bigg/ \left(\sum_{j \neq i}^{N_s} \chi_j / D_{ij}\right). \tag{10}$$

The binary diffusivity D_{ij} between species i and j is obtained through the use of the Chapman–Enskog theory in conjunction with the Lennard–Jones intermolecular potential energy functions [40].

2.3. Gas model

To close the system of Equation (1), the equation of state must be defined. The macroscopic thermodynamic properties of the real gas are described by the general equation of state.

$$p = p(\rho, e, \rho_1, \rho_2, \ldots, \rho_{N_s - 1}). \tag{11}$$

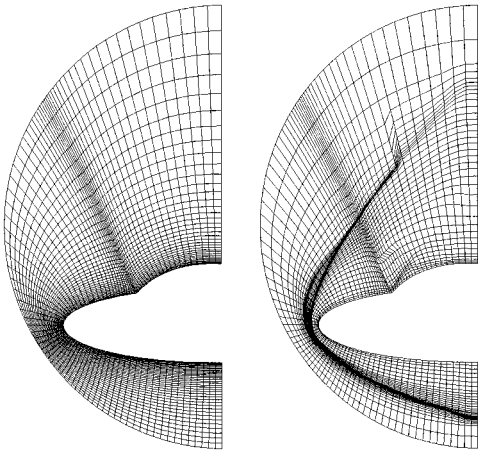

Figure 1. An 89×37 grid for double ellipse (original and adaptive grid).

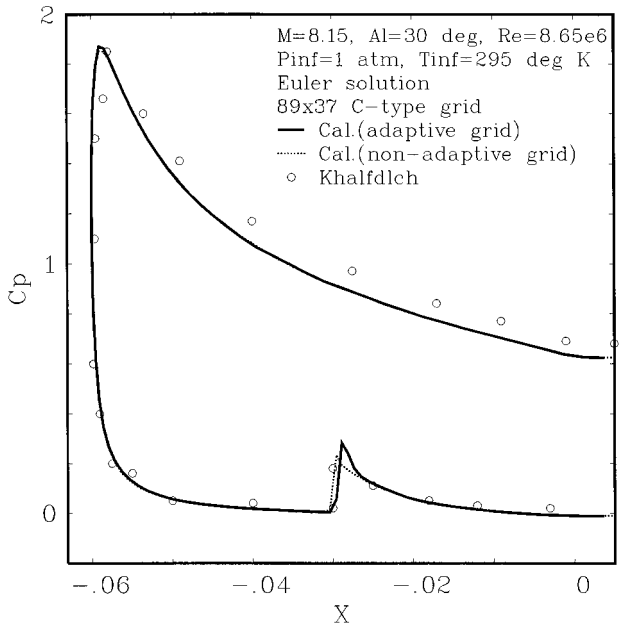

Figure 2. Pressure coefficients along the surface for double ellipse.

Since the total mass density is already included as an independent variable, only $N_s - 1$ species are independent for a chemical system of N_s species. If the intermolecular forces and the volume occupied by molecules are assumed to be negligible, the gas mixture pressure $\tilde{p}$ may be expressed as the sum of the partial pressure due to each species in the ideal gas relation:

$$\tilde{p} = R_u \tilde{T} \sum_i \frac{\tilde{\rho}_i}{W_i}, \tag{12}$$

where R_u is the universal gas constant. The total internal energy of the reacting air can be combined from the internal energy of each species. The internal energy per unit mass of species i may be written as

$$\tilde{e}_i = \frac{3}{2}\frac{R_u}{W_i}\tilde{T} + \tilde{h}_f^0 \tag{13}$$

for monatomic species and

$$\tilde{e}_i = \frac{5}{2}\frac{R_u}{W_i}\tilde{T} + \tilde{e}_{vi} + \tilde{h}_f^0 \tag{14}$$

for diatomic species. $\tilde{e}_{vi}$ is the vibration energy, and can be written as $\tilde{e}_{vi} = \tilde{e}_{vi}(T) = R_i\tilde{\theta}_{vi}/(\exp(\tilde{\theta}_{vi}/\tilde{T}) - 1)$. R_i $(= R_u/W_i)$ is the gas constant of each species, $\tilde{\theta}_{vi}$ is the characteristic vibrational temperature [38] and $\tilde{h}_f^0$ is the heat of formation of each species.

The internal energy of mixture of species $\tilde{e}(= \Sigma_{i=1}^{N_s} Y_i\tilde{e}_i)$ is a function of $\tilde{\rho}$, $\tilde{\rho}_i$ and $\tilde{T}$. If the densities of species are known, the non-linear algebraic equation can be reduced to $\tilde{e} = \tilde{e}(T)$ only.

The flux splitting formulation of the real gas mixture requires the definition of the speed of sound $\tilde{a}$, the specific heat ratio γ and the derivatives of pressure with respect to other independent variables [2,3]. The exact formulation of these derivative is quite complicated for flows involving real gas with non-equilibrium chemistry. Present work employs the concept of

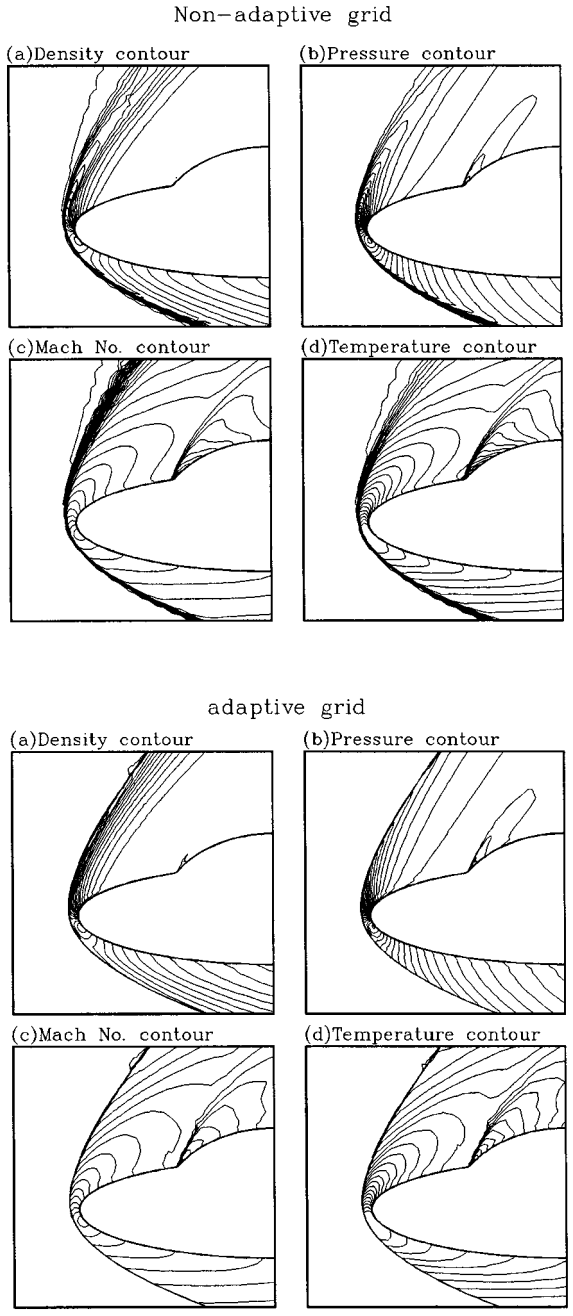

Figure 3. Temperature, Mach number, density and pressure contours for double ellipse.

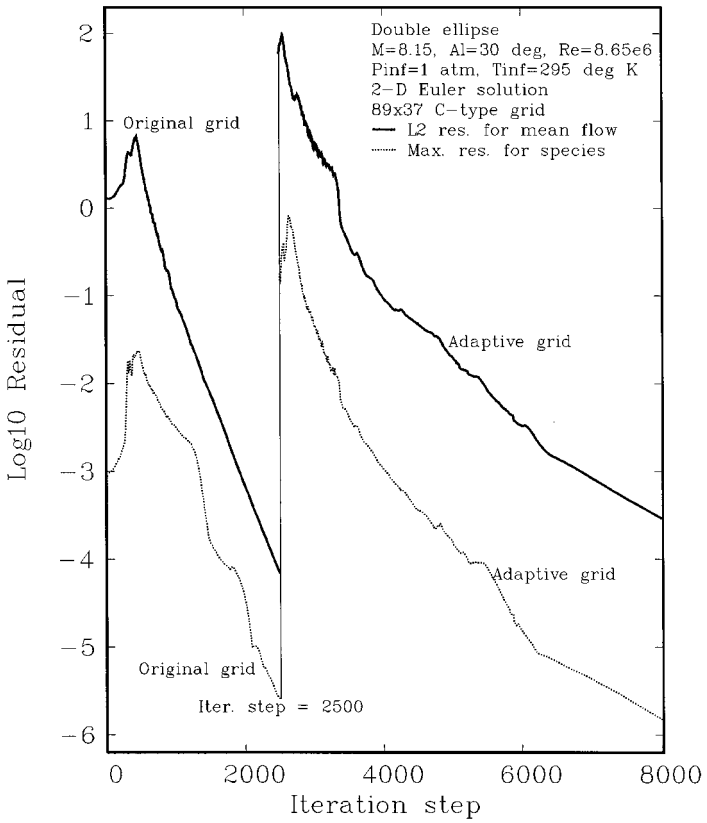

Figure 4. Convergent histories for double ellipse.

'equivalent γ' [1,10] which is in a much simpler formulation. The specific heat ratio γ is defined by $1+\tilde{p}/(\tilde{\rho}\tilde{e})$ and the equivalent sound speed $\tilde{a}^2$ is equal to $\gamma\tilde{p}/\tilde{\rho}$ in this method.

2.4. Chemistry model

For a set of N_R elementary reactions involving N_s species, the rate equations can be written in the general form

$$\sum_{j=1}^{N_s} v'_{mj} n_j \leftrightarrow \sum_{j=1}^{N_s} v''_{mj} n_j, \quad m = 1, 2, \ldots, N_R, \tag{15}$$

where v'_{mj}, v''_{mj} are the stoichiometric coefficients for species j appearing as a reactant in the mth forward and backward reactions respectively, and n_j is the molar concentration for species j ($n_j = \rho_j / W_j$). Also, $k_{\mathrm{f},m}$, $k_{\mathrm{b},m}$ are the forward and backward rate constants for the mth reaction step. $k_{\mathrm{f},m}$, $k_{\mathrm{b},m}$ generally are only the function of temperature. The rate of change of molar concentration of species j by reaction step m is

$$(\dot{n}_j)_m = (v'_{mj} - v''_{mj}) \left(k_{\mathrm{f},m} \prod_{l=1}^{N_s} n_l^{v'_{ml}} - k_{\mathrm{b},m} \prod_{l=1}^{N_s} n_l^{v''_{ml}} \right). \tag{16}$$

The total rate of change of species densities of species j is

$$S_j = W_j \sum_{m=1}^{N_R} (\dot{n}_j)_m = W_j \sum_{m=1}^{N_R} (v'_{mj} - v''_{mj}) \qquad \left(k_{\mathrm{f},m} \prod_{l=1}^{N_s} n_l^{v'_{ml}} - k_{\mathrm{b},m} \prod_{l=1}^{N_s} n_l^{v''_{ml}} \right). \tag{17}$$

It is the source term for species j due to chemical reactions.

2.4.1. Five-species model. In this study, three chemical reaction models are considered. The first is the five-species model which includes five species (N, O, NO, O_2, N_2) and 17 reactions for the dissociation and recombination of air. The forward reaction rate constants for this model are provided by Dunn and Kang [35], except those for the ions and free electrons. The equilibrium rate constants $k_{c,m}$ are given in Vincenti & Kruger [38]. The backward rate constants $k_{\mathrm{b},m}$ can be evaluated by $k_{\mathrm{b},m} = k_{\mathrm{f},m}/k_{c,m}$.

The five elementary chemical reactions of the five-species model in this study are

$$\begin{aligned}
&\text{reaction 1: } N_2 + M \leftrightarrow 2N + M \\
&\text{reaction 2: } O_2 + M \leftrightarrow 2O + M \\
&\text{reaction 3: } NO + M \leftrightarrow N + O + M \\
&\text{reaction 4: } N_2 + O \leftrightarrow NO + N \\
&\text{reaction 5: } NO + O \leftrightarrow O_2 + N
\end{aligned} \tag{18}$$

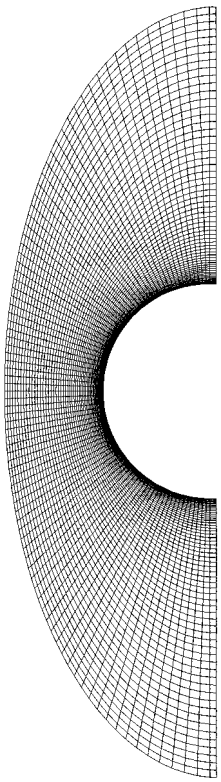

Figure 5. A 91×61 grid for half cylinder.

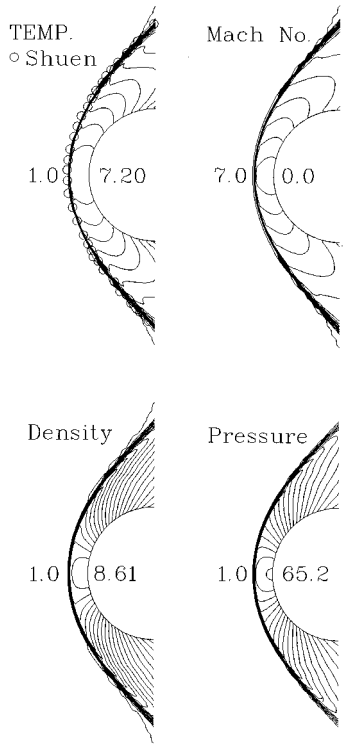

Figure 6. Temperature, Mach number, density and pressure contours for flow over a half cylinder by the five-species model.

The impacting body labelled M can be any one of the five species.

2.4.2. Eleven-species model. The 11-species model proposed by Park [36] utilizes 11 species N, O, NO, O_2, N_2, N^+, O^+, NO^+, O_2^+, N_2^+, e^-, with 47 reactions [36]. The rate constant is also given by Park [36].

2.4.3. Equilibrium model. In the equilibrium model, the air is composed of five species (N, O, NO, O_2, N_2) and three independent equilibrium equations are involved

$$\begin{aligned} &N_2 \rightarrow 2N \\ &O_2 \rightarrow 2O \\ &N_2 + O_2 \rightarrow 2NO. \end{aligned} \tag{19}$$

The law of mass action is thus expressed as follows:

$$\begin{aligned} &\frac{Y_O^2}{Y_{O_2}} = \frac{k_{c,O_2} W_O^2}{\rho W_{O_2}} \\ &\frac{Y_N^2}{Y_{N_2}} = \frac{k_{c,N_2} W_N^2}{\rho W_{N_2}} \\ &\frac{Y_{NO}^2}{Y_{O_2} Y_{N_2}} = \frac{k_{c,NO} W_{NO}^2}{W_{O_2} W_{N_2}} \end{aligned} \tag{20}$$

where k_{c,N_2}, k_{c,O_2}, $k_{c,NO}$ are the function of temperature and are given in Reference [38]. The mass fractions satisfy two additional algebraic equations:

$$Y_N + Y_O + Y_{NO} + Y_{O_2} + Y_{N_2} = 1 \tag{21}$$

$$79\left(\frac{Y_O}{W_O} + \frac{Y_{NO}}{W_{NO}} + \frac{2Y_{O_2}}{W_{O_2}}\right) = 21\left(\frac{Y_N}{W_N} + \frac{Y_{NO}}{W_{NO}} + \frac{2Y_{N_2}}{W_{N_2}}\right). \tag{22}$$

From Equation (22), the ratio of oxygen atoms and nitrogen atoms is a constant (i.e. 21:79). The mass fractions are obtained by Equations (20)–(22).

3. NUMERICAL ALGORITHM

3.1. Spatial differencing

The difference equations are formulated by the finite volume approach in the fully implicit form from Equation (1):

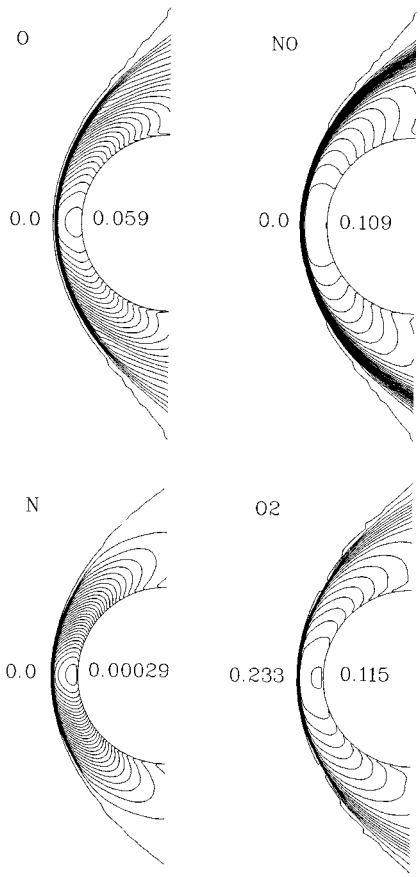

Figure 7. Major species mass fraction contours for flow over a half cylinder by the five-species model.

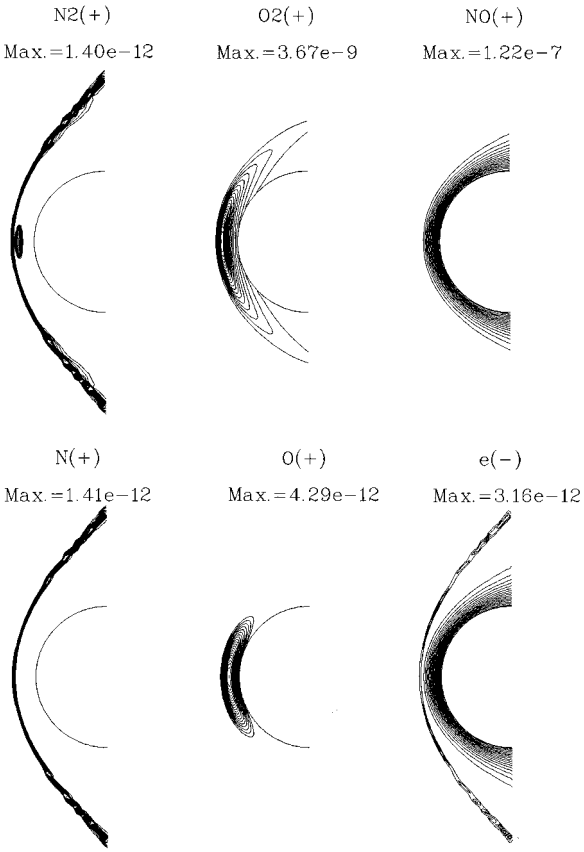

Figure 8. Mass fraction contours for ions and electrons for flow over a half cylinder by the 11-species model.

$$\hat{Q}_{i,j}^{n+1} - \hat{Q}_{i,j}^{n} = -\frac{\Delta t}{\Delta \xi}\left[(\bar{E}-\bar{E}_v)_{i+1/2,j} - (\bar{E}-\bar{E}_v)_{i-1/2,j}\right]^{n+1}$$

$$-\frac{\Delta t}{\Delta \eta}\left[(\bar{F}-\bar{F}_v)_{i,j+1/2} - (\bar{F}-\bar{F}_v)_{i,j-1/2}\right]^{n+1} + \Delta t \hat{S}_{i,j}^{n+1}. \tag{23}$$

Van Leer flux vector splitting scheme [3] is applied for the differencing of the convective term and the central difference scheme is used for the viscous term. The standard splitting in the ξ-direction is:

$$\bar{E}_{i+1/2,j} = \bar{E}^{+}_{i+1/2,j} + \bar{E}^{-}_{i+1/2,j}. \tag{24}$$

Defining $M_\xi \equiv (u\xi_x + v\xi_y)/(a\sqrt{\xi_x^2 + \xi_y^2})$ gives the local Mach number. For local Mach number greater than 1.0, $\bar{E}^{+}_{i+1/2,j} = \bar{E}_{i+1/2,j}$, $\bar{E}^{-}_{i+1/2,j} = 0$. For a local Mach number less than -1.0, $\bar{E}^{-}_{i+1/2,j} = \bar{E}_{i+1/2,j}$, $\bar{E}^{+}_{i+1/2,j} = 0$. In the local subsonic region, $M_\xi^2 < 1$.

The split mass, momentum, energy and concentration fluxes are:

$$
\begin{aligned}
\bar{E}_1^{\pm} &= \pm\frac{1}{4}\rho a(M_\xi \pm 1)^2 \\
\bar{E}_2^{\pm} &= \bar{E}_1^{\pm}\left[u - \frac{\hat{k}_x p(2a \pm u_\xi)}{\rho a^2}\right] \\
\bar{E}_3^{\pm} &= \bar{E}_1^{\pm}\left[v - \frac{\hat{k}_y p(2a \pm u_\xi)}{\rho a^2}\right] \\
\bar{E}_4^{\pm} &= \bar{E}_1^{\pm} H \\
\bar{E}_5^{\pm} &= \bar{E}_1^{\pm} Y_1 \\
\bar{E}_{N_s+3}^{\pm} &= \bar{E}_1^{\pm} Y_{N_S-1}
\end{aligned} \tag{25}
$$

where

$$
H \equiv (E_t + p)/\rho, \qquad u_\xi \equiv u\hat{k}_x + v\hat{k}_y
$$

$$
\hat{k}_x = \frac{\xi_x}{\sqrt{\xi_x^2 + \xi_y^2}}, \qquad \hat{k}_y = \frac{\xi_y}{\sqrt{\xi_x^2 + \xi_y^2}}.
$$

The split fluxes in the η-direction can be similarly obtained. The flow variable in the cell interface $i+1/2$ is evaluated by second-order MUSCL approach. Second-order Van Leer smooth limiter is adopted to switch smoothly from second- to first-order accuracy in regions of strong gradients.

3.2. Time integration

In the present study, all of the equations, including chemical species transport equations, are simultaneously solved. The implicit unfactored backward Euler scheme for the full Navier–Stokes equations and chemically reacting species transport equations which use upwind differencing in the ξ- and η-direction can be written in the form [20]:

$$
\begin{aligned}
&\left[I + \Delta t\left(\frac{\partial \hat{A}^+}{\partial_\xi{}^-} + \frac{\partial \hat{A}^-}{\partial_\xi{}^+} + \frac{\partial \hat{B}^+}{\partial_\eta{}^-} + \frac{\partial \hat{B}^-}{\partial_\eta{}^+}\right) - \Delta t_{\text{chem}}\hat{G}\right]^n \Delta\hat{Q}_{i,j}^n \\
&= -\frac{\Delta t}{\Delta\xi}\left[(\bar{E} - \bar{E}_v)_{i+1/2,j} - (\bar{E} - \bar{E}_v)_{i-1/2,j}\right] - \frac{\Delta t}{\Delta\eta}\left[(\bar{F} - \bar{F}_v)_{i,j+1/2} - (\bar{F} - \bar{F}_v)_{i,j-1/2}\right] \\
&\quad + \Delta t_{\text{chem}}\hat{S}_{i,j},
\end{aligned} \tag{26}
$$

where $\hat{A}^{\pm}, \hat{B}^{\pm}$ are the positive and negative splitting Jacobian matrices in the ξ- and η-directions. Generally, in order to maintain the stability of the thin-layer viscous term, the split Jacobian matrices $\hat{A}^{\pm}, \hat{B}^{\pm}$ are modified as follows which was originally suggested by Coakley [41],

$$
\hat{A}^{\pm} = \hat{R}_\xi(\hat{\lambda}_\xi^{\pm} \pm \bar{\nu}_\xi\hat{I})\hat{R}_\xi^{\pm}; \qquad \hat{B}^{\pm} = \hat{R}_\eta(\hat{\lambda}_\eta^{\pm} \pm \bar{\nu}_\eta\hat{I})\hat{R}_\eta^{\pm}; \tag{27}
$$

$$
\bar{\nu}_\xi = \frac{2\gamma M_\infty(\mu/\rho)|\vec{\nabla}\xi|^2}{(Re_\infty Pr)}. \tag{28}
$$

The source term $\hat{S}$ can be very large and cause the equation set to be stiff. To mitigate the stiff problem, the chemical source terms are treated implicitly. The complete derivation of the source term Jacobian matrix $\hat{G}$ can be found in [3]. The matrix $\hat{G}(=\partial\hat{S}/\partial\hat{Q})$ has $(N_s+3)\times 4$ non-zero elements and the values of these elements may be positive or negative and very large if the time step is large enough. It is possible that the matrix $\hat{G}$ diminishes the diagonal values

of the LHS matrix system and the total matrix system may be unstable. In the present study, a special integration time step for the chemical reaction source term (called Δt_{chem}) is employed. Δt_{chem} is defined by $\text{CFL}_{\text{chem}} \cdot \Delta t_{\text{CFL,chem}}$ where $\Delta t_{\text{CFL,chem}}$ is the approximate CFL-like time scale for total reactions and is defined below:

$$\Delta t_{\text{CFL,chem}} = 1.0/\max(|\hat{G}_{ij}|). \tag{29}$$

CFL_{chem} ranges between 3 and 20. Therefore, the ratio of Δt_{chem} and Δt can be selected with the range of 0.01–1.

The matrix Equation (26) can be replaced by the non-factored form list below:

$$\bar{A}_{i,j}(\Delta Q)_{i-1,j} + \bar{C}_{i,j}(\Delta Q)_{i+1,j} + \bar{E}_{i,j}(\Delta Q)_{i,j-1} + \bar{F}_{i,j}(\Delta Q)_{i,j-1} + \bar{D}_{i,j}(\Delta Q)_{i,j} = \bar{B}_{i,j} \tag{30}$$

$$\bar{D}_{i,j} = \left(\frac{\Delta t}{\text{Vol}_{i,j}}\right)(\hat{A}^{+}_{i+1/2,j} - \hat{A}^{-}_{i-1/2,j} + \hat{B}^{+}_{i,j+1/2} - \hat{B}^{-}_{i,j-1/2}) + I + (\Delta t)\hat{D}_{i,j} \tag{31}$$

$$\bar{A}_{i,j} = -\left(\frac{\Delta t}{\text{Vol}_{i,j}}\right)\hat{A}^{+}_{1-1/2,j}, \qquad \bar{C}_{i,j} = -\left(\frac{\Delta t}{\text{Vol}_{i,j}}\right)\hat{A}^{-}_{1+1/2,j},$$

$$\bar{B}_{i,j} = \frac{\text{RHS of Equation (26)}}{\text{Vol}_{i,j}},$$

$$\bar{E}_{i,j} = -\left(\frac{\Delta t}{\text{Vol}_{i,j}}\right)\hat{B}^{-}_{i,j-1/2}, \qquad \bar{F}_{i,j} = -\left(\frac{\Delta t}{\text{Vol}_{i,j}}\right)\hat{B}^{-}_{i,j+1/2}.$$

Equation (30) forms a block pentadiagonal matrix system of equations, $\mathbf{MX} = \mathbf{B}$, where $\mathbf{M}$ is a $(NI \cdot NJ \cdot (N_s + 3)) \times (NI \cdot NJ \cdot (N_s + 3))$ banded matrix, $\mathbf{X}$ and $\mathbf{B}$ are $(NI \cdot NJ \cdot (N_s + 3))$ column matrices. The coefficient matrix $\bar{A}_{i,j}$, $\bar{C}_{i,j}$, $\bar{D}_{i,j}$, $\bar{E}_{i,j}$, $\bar{F}_{i,j}$ are $(N_s + 3) \times (N_s + 3)$ square matrices and the right hand side matrix $\bar{B}_{i,j}$ is a $(N_s + 3) \times 1$ vector. The unknown $(\Delta Q)_{i,j}$ is conventionally evaluated using block Gauss–Seidel methods with slow convergence. Variant Bi-CG methods were developed in recent years, i.e. CGS [29], Bi-CGSTAB [30], QMR [31] and TFQMR [32]. These methods can significantly simplify the programming and speed up convergence.

The convergence rate of the conjugate gradient methods depends on the eigenvalue distribution of the coefficient matrix. Instead of solving the original linear system $\mathbf{MX} = \mathbf{B}$, the preconditioned conjugate gradient method solves a related linear system, $\mathbf{K}^{-1}\mathbf{MX} = \mathbf{K}^{-1}\mathbf{B}$. The matrix production of $\mathbf{K}^{-1}\mathbf{M}$ has a more favorable eigenspectrum distribution than $\mathbf{M}$, i.e. the eigenvalues are more clustered. The choice of the preconditioner in the present study is based on incomplete factorization of matrix $\mathbf{M}$ which consists of a block lower triangular matrix $\mathbf{L_M}$ a block upper triangular matrix $\mathbf{U_M}$, and a block diagonal matrix $\mathbf{D_M}$, satisfying $\mathbf{M} = (\mathbf{L_M} + \mathbf{D_M})\mathbf{D_M}^{-1}(\mathbf{U_M} + \mathbf{D_M}) + \mathbf{E_M}$, where $\mathbf{E_M}$ is the deviation matrix. The deviation matrix $\mathbf{E_M}$ is often very sparse itself. This factorization method is called incomplete line LU factorization, and is denoted by ILU. Preconditioning with ILU is carried out by choosing $\mathbf{K} = (\mathbf{L_M} + \mathbf{D_M})\mathbf{D_M}^{-1}(\mathbf{U_M} + \mathbf{D_M})$ [42], where $\mathbf{D_M}$ is slightly modified.

The algorithm of Bi-CGSTAB methods with ILU as a preconditioner is applied in the present work and described in detail in Reference [30]. The application of the present method implies the solution of $\mathbf{K}^{-1}\mathbf{MX} = \mathbf{K}^{-1}\mathbf{B}$, but the LU methods solve $\mathbf{KX} = \mathbf{B}$.

However, the numerical stability is sustained with difficulty due to stiff source terms of chemical reactions. Some relaxation procedures for integrating species transport equations are needed, as Palmer [13] suggested.

3.3. Testing problems and boundary/initial conditions

Numerical computations have been performed for hypersonic flow past (1) a double ellipse body at a 30° angle of attack for the freestream condition of $M_\infty = 8.15$, $p_\infty = 1$ atm, $T_\infty = 300$ K and $Re_\infty = 8.8 \times 10^6$ [43]; (2) a half cylinder at a zero angle of attack for the freestream condition of $M_\infty = 7.0$, $p_\infty = 1$ atm, $T_\infty = 600$ K and $Re_\infty = 6 \times 10^6$ [14]; (3) a blunt body made of a cylindrical portion followed by planes with a 15° inclination [10]. The freestream conditions are taken to correspond approximately to the standard atmosphere at the altitude of 75 km ($M_\infty = 25.0$, $p_\infty = 2.52$ Pa, $T_\infty = 205.3$ K, $Re_\infty = 1947$). Half-C type grids are generated by the hyperbolic grid-generation scheme. On the $\xi = 1$ and $\xi = \xi_{\max}$ boundary, the supersonic outflow condition is employed. On $\eta = \eta_{\max}$ boundary, supersonic inflow condition is specified. An adiabatic wall boundary is applied on the $\eta = 1$ boundary, and the no-slip condition and zero normal pressure and concentration gradient are imposed on the wall.

Uniform flow fields of freestream conditions for mean flow equations and species are assumed to be in the equilibrium state. For the five-species model calculation, the equilibrium species fractions of freestream conditions can be solved from the chemical rate equations. For 11-species model computation, The mass fractions of N_2 and O_2 are initially set to 0.7667 and 0.2333, and the mass fractions of other species are assumed to be very small (i.e. 10^{-15}).

3.4. Mesh adaptation

The mesh must be refined locally in order to increase the spatial resolution in the nearby region, because the shock induces the dissociation phenomena. The moving grid method of Dwyer [44,45] is employed in the present study. The mathematical expression for the technique is, for any interval

$$W_i \Delta X_i = \text{constant},$$

where W_i is the weighting function of the ith interval. As the value of weighting function becomes greater, the corresponding interval becomes smaller. Thus, by constructing the weighting function according to the gradient of the dependent variables, the grid can cluster near the region where the solution variation is large. W is assumed as $1 + \Sigma_k b_k |\partial \phi_k / \partial s|$, where ϕ_k's are dependent variables and b_k's are the 'normalizing factors'. For this study, the mesh adaptation is executed only in the η-direction, and a smoothing procedure is employed to produce regular meshes.

4. RESULTS AND DISCUSSIONS

The first testing problem is hypersonic flow past a double ellipse blunt body. The configuration of the body and grid is shown in Figure 1. The grid is constructed as a 89×37 half-C grid and the first grid line in the normal direction is at a distance 0.0005 off the wall, (the maximum diameter of the double ellipse is 0.06). The restructured grid is constructed by clustering the grid line in the η-direction at the bow shock region and the attach shock region, near the discontinuous location on the leeside surface. The restructure, based on the converged solution of the flowfield, employed the original grid (iteration step = 2500). The solution is then interpolated onto the new adaptive grid and the time integration for this case proceeds. The surface pressure coefficients computed along windward and leeward surface are plotted in Figure 2. The computed pressure distribution on the leeward side of the present method is

compared with that of Khalfdlch [42]. The shock is obvious at the location $X = -0.03$. The adaptive grid solution yields a better resolution than the original grid solution. The computed distribution on the windward side is 5% lower than Khalfdlch's prediction. The temperature, Mach number, density and pressure contours (Figure 3) indicate that the bow shock resolution is apparently improved by mesh adaptation, especially in the leeside region. The calculated shock position in the present study gives the same result as Esser [42].

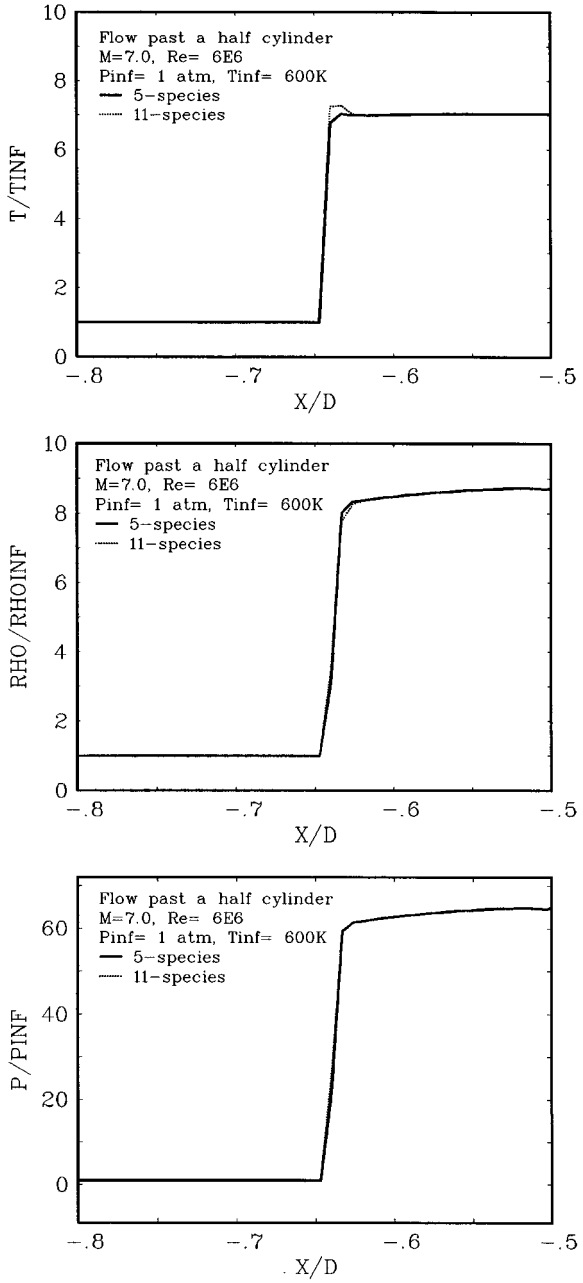

Figure 9. Distributions of physical quantities along the stagnation streamline for flow over a half cylinder.

Table 1. The comparisons of stagnation properties for flow past a half cylinder

Stagnation properties	Pre. (five-species)	Pre. (11-species)	Shuen
p (atm)	65.0	65.0	63.0
T (K)	4224	4221	4260
Y_N	0.000244	0.000243	0.00024
Y_O	0.0608	0.0608	0.065
Y_{NO}	0.102	0.102	0.102
Y_{O_2}	0.118	0.118	0.121

The convergent histories are plotted in Figure 4. The L_2 residuals of mean flow and maximum average residuals for all species equations used the new adaptive grid, which can be reduced smoothly by five and six orders, within 5500 iteration numbers (i.e. from iteration step 2500 to 8000). The maximum CFL number is 10.0. The definition of 'maximum average residual' is the summation of normalized maximum residual of all species. The convergent characteristics of the species equations can be displayed by this residual.

The second testing problem is a hypersonic flow past a half cylinder. The 91×61 grid network is shown in Figure 5. The first grid line in the normal direction is at a distance 0.0015 D off the wall. Five-species and 11-species chemical reaction models of air dissociation are employed. The calculations by the five-species model repeated the work of Shuen [14]. The

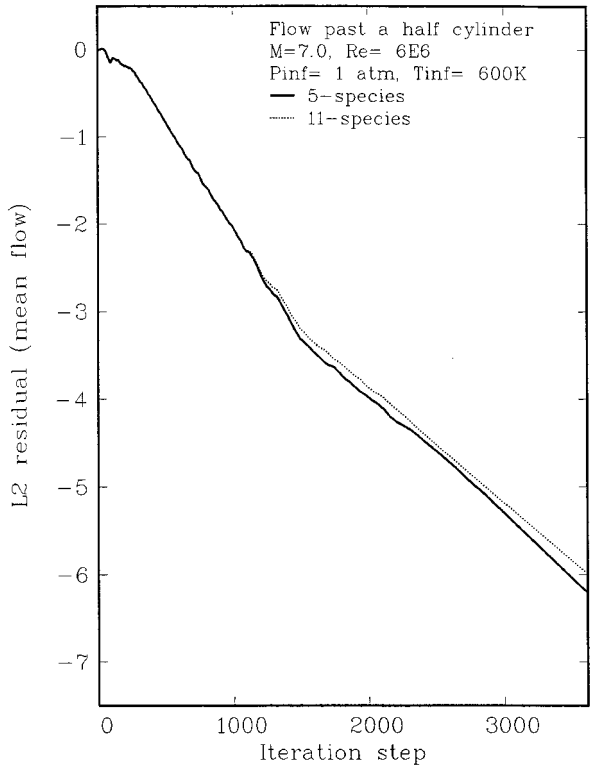

Figure 10. L_2 residuals of mean flow equations by different chemical reaction models for flow over a half cylinder.

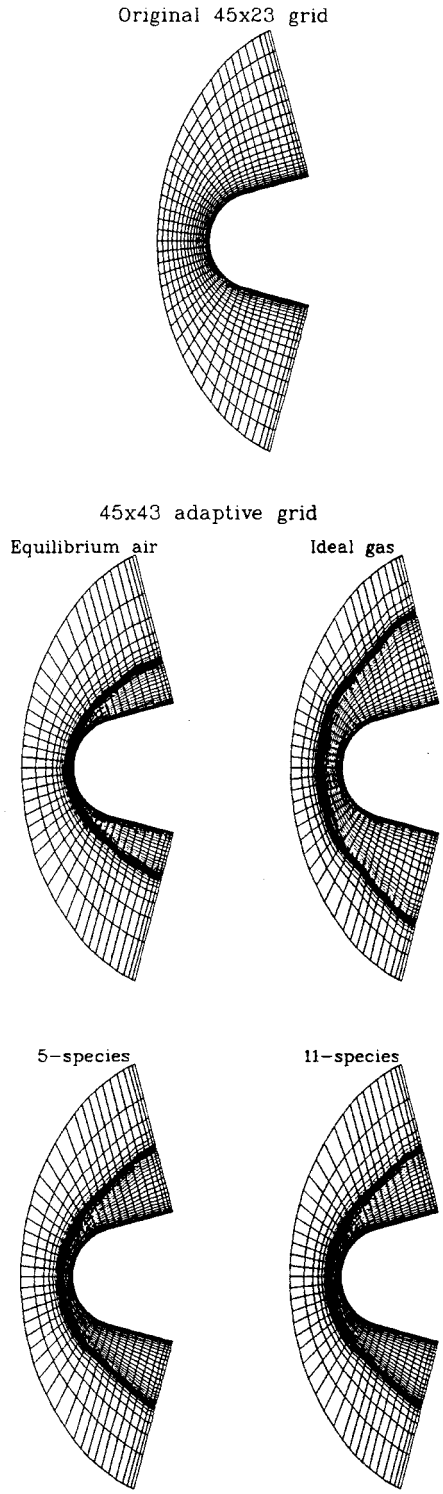

Figure 11. A 45×23 original grid and four 45×43 adaptive grids for a 2-D blunt body.

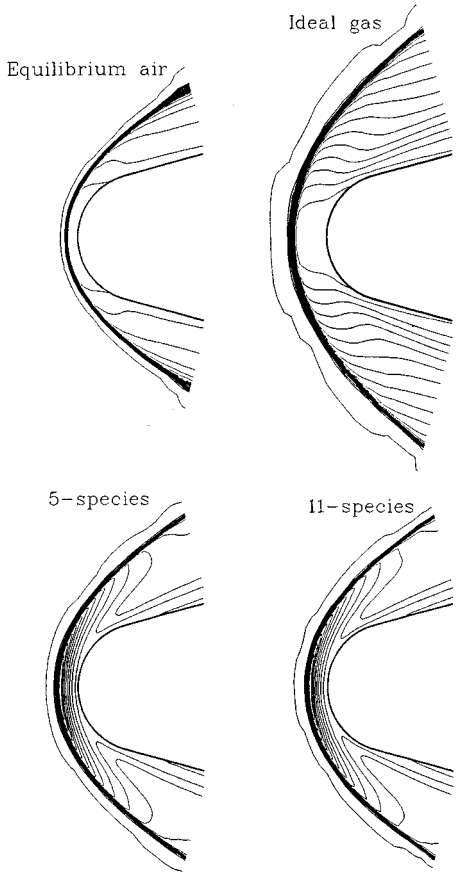

Figure 12. Temperature contours for flow over a 2-D blunt body by ideal gas and three chemical reaction models.

major difference between the present work and Shuen's is the formulation of flux vector splitting. Shuen's method requires the evaluation for frozen sound speed and pressure derivatives p_e, p_ρ and $p_{\rho i}$, but the present work employed the simplified 'equivalent γ and sound speed' formulations. The present results of the five-species model are almost identical to those of Shuen [14].

Figure 6 plots the contours of density, Mach number, pressure, and temperature by the five-species chemical reaction model. It can be seen that the temperature contours are very similar to those of Shuen (see Reference [14], Figure 1). The stagnation properties of temperature and pressure of this test case are obtained as 4224 K and 65.0 atm in the present computation, while Shuen found values of 4260 K and 63 atm.

Figure 7 shows the mass fraction contours of species N, O, NO and O_2 by the five-species chemical reaction model. The contour maps are very similar to those of Shuen (see Reference [14], Figure 2). The computed mass fractions of these four species at the stagnation point by the present computation are 0.000244, 0.0608, 0.102 and 0.118, and the values found by Shuen are 0.00024, 0.065, 0.102 and 0.121. The maximum difference is 6%. The contours of density, Mach number, pressure, temperature and the mass fraction of species N, O, NO, O_2 by the 11-species chemical reaction model are very similar to those by the five-species model. In order to reduce the length of the paper, these contours are not shown. The mass fraction contours

of ions N_2^+, O_2^+, NO^+, N^+, O^+ and electron e^- are shown in Figure 8. The maximum mass fraction of these six species is of the order 10^{-7}. It implies that electrons and ions are generated at the bow shock.

Figure 9 compares the temperature, pressure and density obtained by five-species and 11-species models on the stagnation streamline. It shows that the temperature, pressure and density after the bow shock and the stand-off distance are almost identical for both models. It indicates the rare ionization due to the low peak temperature of 4226 K. The detailed properties at the stagnation point are listed in Table 1.

The convergence histories are illustrated in Figure 10. The L_2 residual for mean flow equations can be reduced by seven orders for both reaction models within 3600 iteration steps. The maximum CFL number used for both case is set to be 40. The code efficiency is similar to Shuen's work [14].

The third test case is the flow past a cylindrical blunt body with a Mach number of 25. The 45×23 grid (Figure 11), with minimum spacing of 0.005 D in the normal direction, is used to

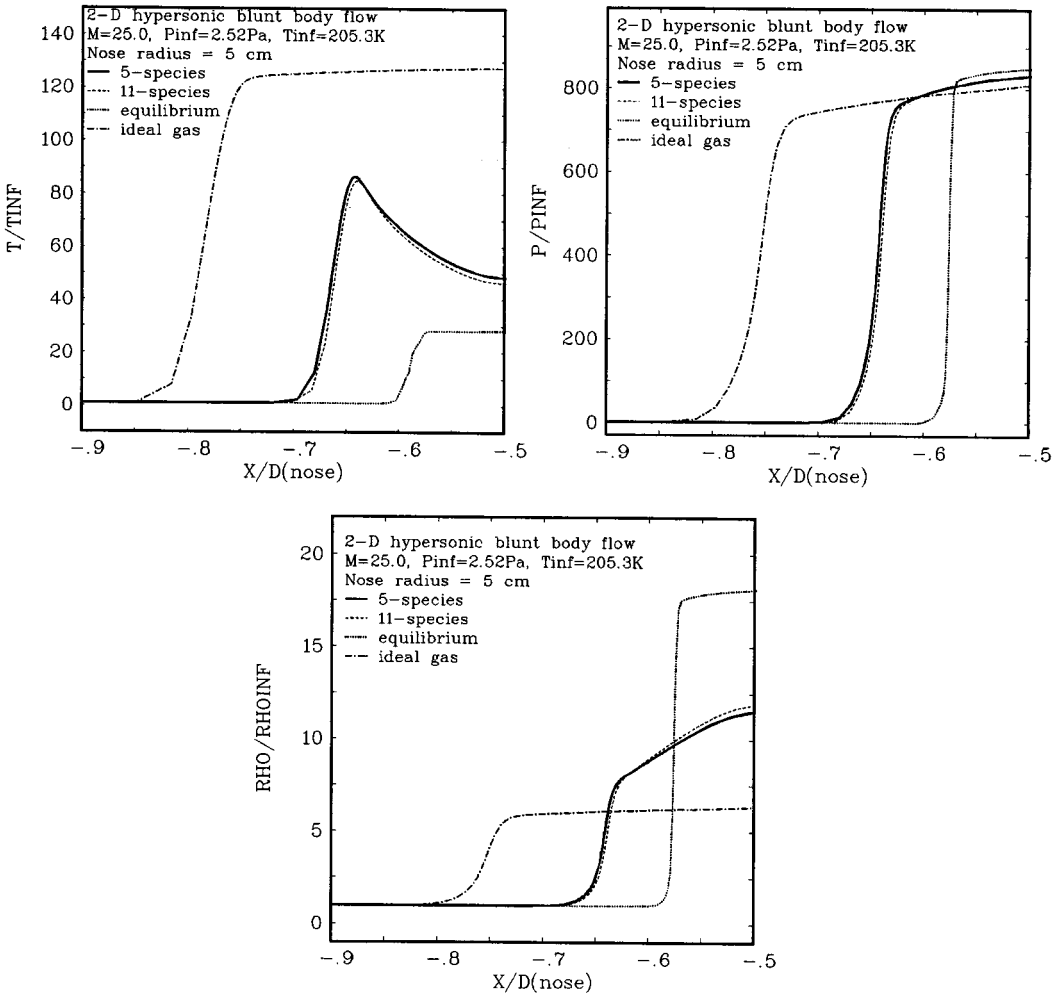

Figure 13. Distributions of physical quantities along the stagnation streamline for flow over a 2-D blunt body.

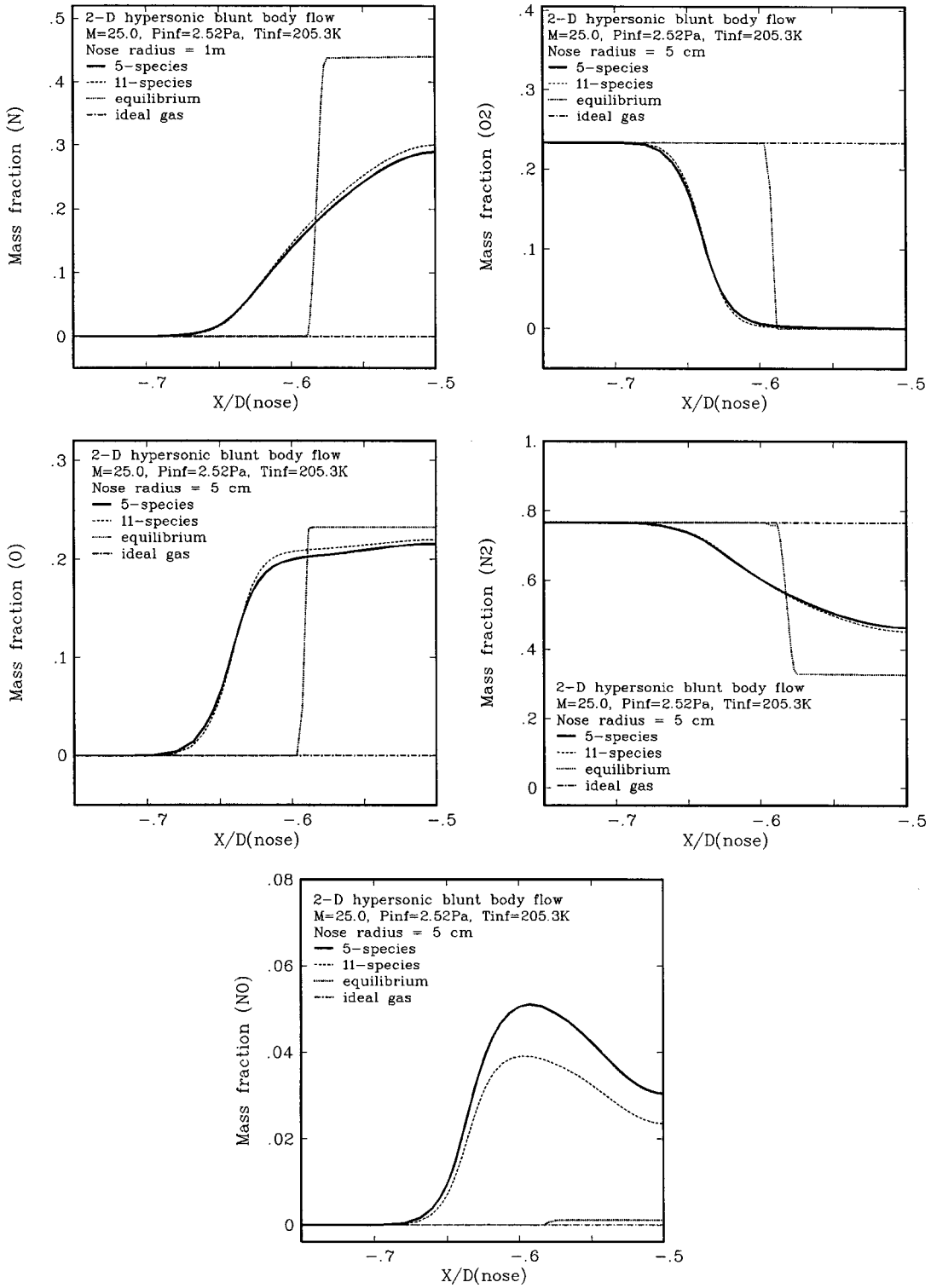

Figure 14. Distributions of mass fractions of major species along the stagnation streamline for flow over a 2-D blunt body.

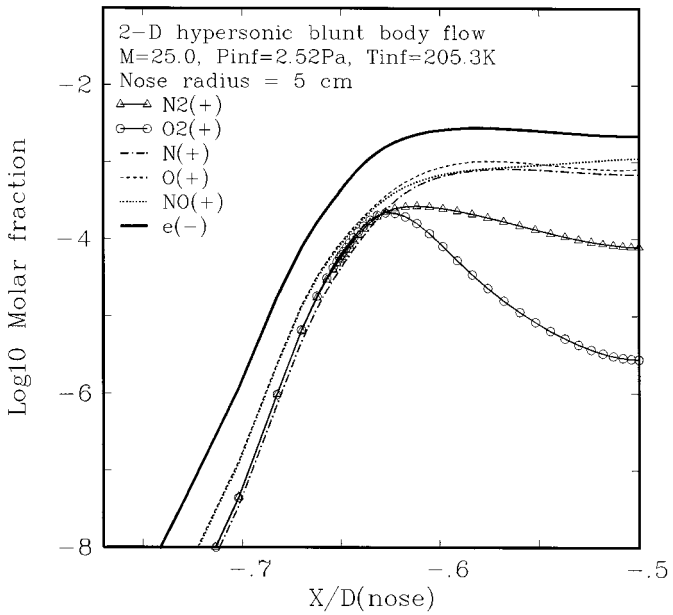

Figure 15. Distributions of molar fractions of ions and electrons along the stagnation streamline for flow over a 2-D blunt body.

obtain the original coarse-grid solution. Next, the fine adaptive grid with grid nodes of 45×43 is constructed (Figure 11). The computations are carried out using this restructured grid from a time of zero. Four reaction models are employed for this problem: five-species and 11 species non-equilibrium reaction models, equilibrium model and ideal gas model. The iso-temperature plot is shown in Figure 12. The ideal gas model calculation gives the highest stagnation temperature 25841 K. This value is approaches the value obtained from the simple formula for stagnation property, i.e. $T_{\text{stag}} = T_\infty(1 + 0.2M_\infty^2) = 25868$ K. The equilibrium model gives the lowest stagnation temperature, i.e. 5794 K, and the temperature is almost constant in the region between the blunt nose and bow shock. The contour maps and the shock stand-off distance are similar for both non-equilibrium models, the stagnation temperature by 11-species model (9958 K) is slightly higher than that of the five-species model (9519 K). Although the mesh adaptation technique is included, the shock resolutions for these reaction models are not sharp because the viscous effect is apparent for the freestream Reynolds number of 1947.

The stand-off distances by four models can be measured as $0.16R$, $0.34R$, $0.34R$ and $0.54R$ from Figure 13 for equilibrium, five-species and 11-species non-equilibrium and ideal gas model respectively. The peak temperatures behind the shock are 17729 K for five-species and 17404 K for 11-species non-equilibrium model. The temperature is reduced gradually to a stagnation temperature which is higher than those of equilibrium and the five-species non-equilibrium model. The peak pressure is almost the same for three models. The mass fractions of the major constituents of the gas on the stagnation streamline are plotted in Figure 14. These plots illustrate the degree of chemical non-equilibrium in the flow field for these models. For the equilibrium model, the dissociation of N_2 and O_2 is sharply behind the bow shock, but for the non-equilibrium reaction models, the dissociation cannot proceed as rapidly when the bow shock is formed and the temperature behind the shock rises. The mass fraction of NO behind the bow shock exhibits the maximum difference for both non-equilibrium reaction models. The

mass fraction of NO which is increased at the bow shock for the five-species model is apparently larger than that of 11-species models, because the 11-species non-equilibrium model includes additive ionization reactions but the five-species does not. The differences in mass fraction NO for both non-equilibrium models are due to ionization process. Figure 15 is a plot of the molar concentration of the ions and electrons on the stagnation streamline.

The convergent histories for mean flow and species equations are plotted in Figure 16. The L_2 residual for mean flow equations can be reduced by five orders for three reaction models within 5000 iteration steps. The local time step is adopted and the maximum reference time step value is set to be 0.001 for the adaptive mesh. The 11-species non-equilibrium model displays the slowest convergent rate of L_2 residual of species equations.

5. CONCLUSION

A numerical program for solving the non-equilibrium Navier–Stokes equation is proposed and satisfactorily developed. The method is based on a finite volume, Van Leer's flux vector splitting spatial discretization, and is integrated by an implicit unfactored method with preconditioning Bi-CGSTAB algorithm matrix solvers. Five-species and 11-species air dissociation chemical models, as well as ideal gas model and equilibrium gas model are included in the present work. The test cases demonstrate the good shock-capturing capability as well as the robustness of the convergence, especially through the use of the adaptive grid.

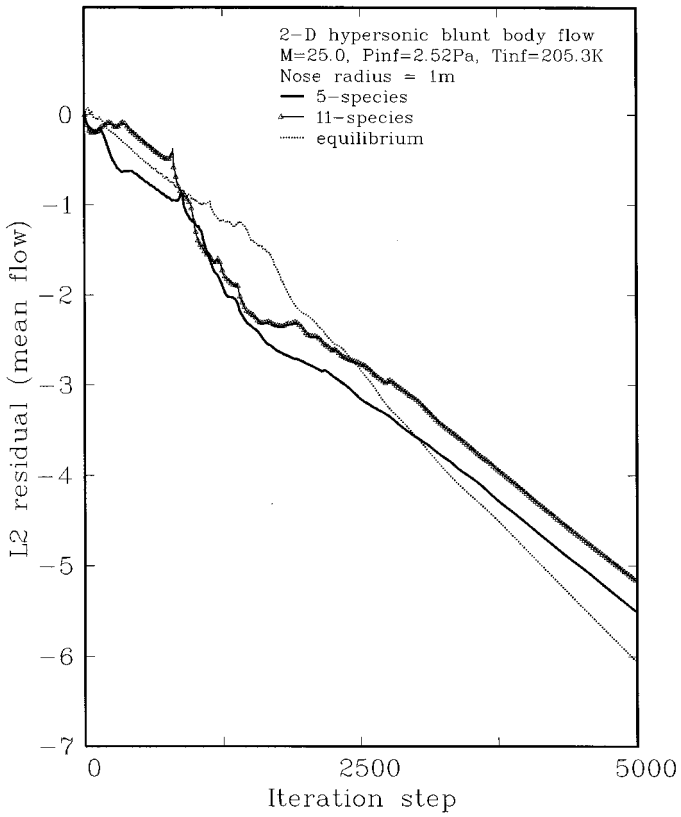

Figure 16. L_2 residuals of mean flow equations by different chemical reaction models for flow over a 2-D blunt body.

REFERENCES

1. B. Grossman and R.W. Walters, 'Analysis of flux-split algorithms for Euler's equations with real gas', *AIAA J.*, **27**, (1989).
2. M.S. Liou, B. Van Leer and J.S. Shuen, 'Splitting of inviscid fluxes for real gas', *J. Comput. Phys.*, **87**, 1–24 (1990).
3. M.S. Liou, B. Van Leer and J.S. Shuen, 'Inviscid flux-splitting algorithms for real gas with non-equilibrium chemistry', *J. Comput. Phys.*, **90**, 371–395 (1990).
4. M. Vinokur and J.-L. Montagne, 'Generalized flux-vector splitting and roe average for an equilibrium real gas', *J. Comput. Phys.*, **89**, 276–300 (1990).
5. M. Vinokur and Y. Liu, 'Equilibrium gas flow computations II. An analysis of numerical formulations of conservation laws', *AIAA Paper No. 88-0127*, 1988.
6. B. Grossman and P. Cinnella, 'Flux-split algorithms for flows with non-equilibrium chemistry and vibrational relaxation', *J. Comput. Phys.*, **88**, 131–168 (1990).
7. J.L. Steger and R.F. Warming, 'Flux vector splitting of the inviscid gasdynamic equations with application to finite difference methods', *J. Comput. Phys.*, **40**, 263–293 (1981).
8. W.K. Anderson, J.L. Thomas and B. Van Leer, 'A comparison of finite volume flux vector splittings for the Euler equations', *AIAA Paper 85-0122*, Jan. 1985.
9. P.L. Roe, 'Approximate Riemann solvers, parameter vectors, and difference schemes', *J. Comput. Phys.*, **43**, 357–372 (1981).
10. J.A. Desideri, 'The computation over unstructed grids of inviscid hypersonic reactive flow by upwind finite volume schemes,' Chapter 11, in T.K.S. Murthy (ed.), *Computational Methods in Hypersonic Aerodynamics*, Computational Mechanics, Southampton/Boston.
11. J.S. Shuen and S. Yoon, 'Numerical study of chemically reacting flows using lower–upper symmetric successive overrelaxation scheme', *AIAA J.*, **27**, 1752–1760 (1989).
12. M. Mani, R.H. Bush and P.G. Vogel, 'Implicit equilibrium and finite rate chemistry models for high speed flow applications', *AIAA Paper No. 91-3299*, 1991.
13. G. Palmer, 'An efficient, explicit finite rate algorithm to compute flows in chemical nonequilibrium', *AIAA Paper 89-0522*, 1989.
14. J.-S. Shuen, 'Upwind differencing and LU factorization for chemical non-equilibrium Navier–Stokes equations', *J. Comput. Phys.*, **99**, 233–250 (1992).
15. C.-P. Li, 'Computational aspects of chemically reacting flows', *AIAA Paper No. 91-1574-CP*, 1991.
16. C. Park and S. Yoon, 'Fully coupled implicit method for thermochemical nonequilibrium air at suborbital flight speeds', *J. Spacecraft Rocket*, **28**, January–Feburary 1991.
17. S.T. Imaly, D.W. Roberts and M. Soetrisno, 'Non-equilibrium thermo-chemical calculations using a diagonal implicit scheme', *AIAA Paper No. 91-0468*, 1991.
18. P.A. Gnoffo, 'Upwind-biased, point-implicit relaxation strategies for viscous, hypersonic flows', *AIAA Paper No. 89-1972-CP*, 1989.
19. G.V. Candler and R.W. MacCormack, 'The computation of hypersonic ionized flows in chemical thermal nonequilibrium', *AIAA Paper No. 88-0511*, 1988.
20. R.W. MacCormack, 'Current status of numerical solutions of the Navier–Stokes equations', *AIAA Paper 85-0032*, AIAA 23rd Aerospace Science Meeting, Reno, Nevada, Jan. 1985.
21. M.R. Hestenes and E. Stiefel, 'Methods of conjugate gradients for solving linear systems', *J. Res. Natl. Burl Stand.*, **49**, 409–436 (1952).
22. R. Fletcher, 'Conjugate gradient methods for indefinite systems', Lecture Notes in Mathematics, Vol. 506, Springer, Berlin, Heidelberg, New York, 1976, pp. 73–89.
23. H.C. Elman, 'Iterative methods for large sparse nonsymmetric systems of linear equations', *Ph.D. Thesis*, Computer Science Dept. Yale University, New Haven. CT, 1982.
24. Y. Saad and M. Schultz, 'GMRES: A generalized minimum residual algorithm for solving nonsymmetric linear systems', *SIAM J. Sci. Stat. Comput.*, **7**, 856–869 (1986).
25. L.B. Wigton, N.J. Yu and D.P. Young, 'GMRES acceleration of computational fluid dynamic codes', *AIAA Paper No. 85-1494-CP*, AIAA 7th Computational Fluid Dynamics Conference, Cincinnato, Ohio, July 1985.
26. S. Obayashi, 'Numerical simulation of underexpanded plumes using upwind algorithms', *AIAA Paper No. 88 4360*, AIAA Atmospheric and Flight Mechanics Conference, Minneapolis, Minnesota, Aug. 1988.
27. V. Venkatakrishnan, 'Preconditioned conjugate gradient methods for the compressible Navier–Stokes equations', *AIAA J.*, **29**, 1092–1100 (1991).
28. K. Ajmani, N., Wing-fai and L. Meng-Sing, 'Generalized conjugate-gradient methods for the Navier–Stokes equations', *AIAA Paper No. 91-1556*, AIAA 10th Computational Fluid Dynamics Conference, Honolulu, Hawaii, June 1991.
29. P. Sonneveld, 'CGS, a fast lanczos-type solver for nonsymmetric linear systems', *SIAM J. Sci. Stat. Comput.*, **10**, 36–52 (1989).
30. H.A. Van Der Vorst, 'Bi-CGSTAB: A fast and smoothly convergent variant of Bi-CG for the solution of non-symmetric linear systems', *SIAM J. Sci. Stat. Comput.*, **13**, 631–644 (1992).

31. R.W. Freund and N.M. Nachtigal, 'QMR: a quasi-minimal residual method for non-hermitian linear systems', *Numer. Math.*, **60**, 315–339 (1991).
32. R.W. Freund, 'A transpose-free quasi-minimal residual method for non-hermitian linear systems', *SIAM J. Sci. Stat. Comp.*, **14**, 470–482 (1993).
33. D.Y. Lin Herng Yang and Ching-Chang Chieng, 'Variant bi-conjugate gradient methods for the compressible Navier–Stokes solver with two equation model of turbulence', *AIAA J.*, **33,** 1177–1184.
34. C.C. Chuang and Ching-Chang Chieng, 'Comparison of variants of the bi-conjugate gradient methods for compressible Navier–Stokes solver with second moment closure', *Int. j. numer. methods fluids*, **17**, 233–253 (1995).
35. S.-W. Kang, M.G. Dunn and W.L. Jones, 'Theoretical and measured electron-density distributions for the ram vehicle at high altitudes', *AIAA Paper No. 72-689*, 1972.
36. C. Park, 'On convergence of computation of chemically reacting flows', *AIAA Paper No. 85-0247*, AIAA 23rd Aerospace Science Meeting, Reno, Nevada, Jan. 1985.
37. F. Blottner, 'Chemical reacting viscous flow program for multi-component gas mixture', *Rep. No. SC-RR70-754*, Sandia Laboratories, Dec. 1991.
38. W.G. Vincenti and C.H. Kruger, *Introduction to Physics Gas Dynamics*, R.E. Krieger, Malabar/Florida, 1982.
39. C.R. Wilke, 'A viscosity equation for gas mixtures', *J. Chem. Phys.*, **18**, 517–519 (1950).
40. R.C. Reid, J.M. Prausnitz and T.K. Sherwood, *The Properties of Gases and Liquids*, 3rd edn, McGraw-Hill, New York, 1977.
41. T.J. Coakley, 'Turbulence modeling methods for the compressible Navier–Stokes equations', *AIAA Paper 83-1693*, AIAA 16th Fluid and Plasma Dynamics Conference, Danvers, Massachusetts, July 1983.
42. T.A. Meijerink and H.A. van der Vorst, 'Guidelines for the usage of incomplete decompositions in solving sets of linear equations as they occur in practical problems', *J. Comput. Phys.*, **44**, 134–155 (1981).
43. J.A. Essers, M. Delanaye and P. Rogiest, 'An upwind-biased finite-volume technique solving compressible Navier–Stokes equations on irregular meshes and shock-boundary layer interactions', *AIAA Paper No. 93-3377-CP*, AIAA 11th Computational Fluid Dynamics Conference, June. 1993.
44. H.A. Dwyer, R.J. Kee and R.B. Sanders, 'An adaptive grid method for problems in fluid mechanics and heat transfer', *AIAA J.*, **18**, (1980).
45. H.A. Dwyer, 'Grid adaptation for problems in fluid mechanics', *AIAA J.*, **22**, (1984).

